Pyrrolidinium-Based Ionic Liquids Doped with Lithium Salts: How Does Li^+ Coordination Affect Its Diffusivity?

Franca Castiglione,[†] Antonino Famulari,[†] Guido Raos,[†] Stefano V. Meille,[†] Andrea Mele,*[,†,‡] Giovanni Battista Appetecchi,[§] and Stefano Passerini[∥,⊥]

[†]Department of Chemistry, Materials and Chemical Engineering "G. Natta", Politecnico di Milano, Piazza L. Da Vinci 32, 20133 Milano, Italy

[‡]CNR − Istituto di Chimica per il Riconoscimento Molecolare, Via L. Mancinelli, 7, 20131 Milano, Italy

[§]ENEA, Agency New Technol Energy & Sustainable Econ Dev, UTRINN IFC, Via Anguillarese 301, I-00123 Rome, Italy

[∥]Helmholtz Institute Ulm (HIU), Electrochemistry I, Helmholtz Strasse 1, 89081 Ulm, Germany

[⊥]Karlsruhe Institute of Technology, P.O. Box 3640, 76021 Karlsruhe, Germany

1. INTRODUCTION

Room-temperature ionic liquids (ILs) are being incorporated as electrolyte materials in a wide variety of electrochemical devices including solar cells, fuel cells, and electrochemical (super or ultra) capacitors because of their favorable properties, such as a wide electrochemical window, high chemical and thermal stability, and negligible vapor pressure.[1−7] In particular, ILs represent a greener and safer alternative to volatile organic liquids as solvents in lithium batteries.[8−10] Several studies have reported that the addition of a lithium salt to an IL leads to an increase in viscosity and often does not produce the desired performance in terms of Li-ion mobility.[11,12] To improve lithium batteries, particularly in terms of current density, it is thus important to clarify the transport properties of IL solutions.

Important structural information on Li-doped ILs has been obtained by nuclear magnetic resonance (NMR) and vibrational spectroscopies.[13−15] Molecular dynamics simulations and ab initio calculations have also been used to clarify Li-ion transport at the molecular level.[16−22] Studies carried out mainly on TFSI-based ILs have demonstrated that the higher viscosities and reduced Li-ion mobilities are due to the aggregation of the anions around the small cation.

In our previous publications we have reported the conductivity and ion diffusion coefficients of neat pyrrolidinium-based ILs and their mixtures, establishing the foundations for a long-term project on the structure and dynamics of ILs of interest for innovative Li-ion batteries (LIB).[14,23−26] In particular, we studied by NMR the binary mixture of *N*-butyl-*N*-methylpyrrolidinium TFSI with LiTFSI of 9 to 1 molar composition. Such composition is poorer in lithium with respect to the eutectic composition found for the 0.85:0.15 mixture.[26] This prevents crystallization of the $PYR_{14}X$:LiX mixture, even at high Li^+ concentration gradient, and provides

Received: September 16, 2014
Revised: November 4, 2014
Published: November 4, 2014

moderate lithium salt concentration resulting in acceptable viscosity. That system showed a unique behavior of the transport properties of Li ions: indeed the activation energy for the diffusion of Li^+ in this mixture was found to be significantly and unexpectedly larger than the corresponding ones for the PYR_{14}^+ and $TFSI^-$ components in the same system. This peculiarity determined the existence of crossover temperatures in the diffusivity values of the components (PYR_{14}^+, $TFSI^-$, and Li^+), namely "temperature values defining the inversion of diffusivity orders of the ions",[14] with remarkable consequences on the corresponding transference numbers and possible implications in battery design. This fact prompted further investigation on whether or not this behavior could be generalized to a larger class of fluorinated anions sharing the sulfonylimide core flanked by variable length perfluorocarbon chains. Moreover, as we postulated[14] that the observed anomalous activation energy trend of Li^+ diffusivity with T might be related to the so-called "structure diffusion" mechanism of Li^+ diffusion, it is our interest to confirm whether or not the Li ion self-diffusion in ILs containing sulfonylimide anions may indeed be subject to a complex mechanism consisting of breaking of coordinative Li-anion bonds, jumping of Li ions to the adjacent anions shell and reformation of Li-anion coordination complex.

Here we present a study of two ionic liquid solutions: *N*-butyl-*N*-methylpyrrolidinium bis(pentafluoroethanesulfonyl)-imide (PYR_{14}BETI) and *N*-butyl-*N*-methylpyrrolidinium (trifluoromethanesulfonyl)-(nonafluorobutanesulfonyl)imide ($PYR_{14}IM_{14}$), doped with the lithium salt sharing the same anion (LiX, X= BETI or IM_{14}). The anions can be considered as higher homologues of TFSI, with symmetric and non-symmetric perfluorinated chains. We have measured the ionic conductivity, the viscosity and the self-diffusion coefficient of each ion by the pulsed gradient spin echo (PGSE) NMR method. The activation energies for these processes have been obtained from their temperature dependence and compared with the data for the neat ILs. Finally, heteronuclear $\{^1H-^7Li\}$ and $\{^1H-^{19}F\}$ Overhauser correlation experiments (HOESY) and density functional theory (DFT) calculations, respectively on the LiX-IL mixtures and on $[Li(X)_2]^-$ complexes, provide atomic-level detail on relevant interionic contacts and processes. In particular, calculations on the formation-disruption of the $[Li(TFSI)_2]^-$ adducts illustrate the processes likely to occur during the structure diffusion mechanism. The combination of experimental and computational results provides a coherent picture of the relationship between the Li-ion environment and the transport properties of the mixtures.

2. EXPERIMENTAL SECTION

2.1. Materials. The PYR_{14}BETI and $PYR_{14}IM_{14}$ ionic liquids were synthesized through a novel procedure developed at ENEA and described in detail elsewhere.[25] The LiBETI (>99.9 wt %, battery grade) salt was purchased from 3M, whereas $LiIM_{14}$ was prepared starting from the aqueous solution of HIM_{14} (60 wt %, kindly provided by 3M) and Li_2CO_3 (99 wt %, Aldrich), which was added in slight excess with respect to the stoichiometric amount. Water was evaporated (from the resulting $LiIM_{14}$ solution) under vacuum at 90 °C and, then, the lithium salt was dissolved in absolute ethanol to allow precipitation of the Li_2CO_3 excess (insoluble in ethanol), which was removed by vacuum filtration. Finally, ethanol was evaporated under vacuum at 70 °C. LiBETI and $LiIM_{14}$ were dried in high vacuum ($<10^{-6}$ mmHg) at 120 °C overnight before experimental measurements. The binary mixtures PYR_{14}BETI/LiBETI and $PYR_{14}IM_{14}/LiIM_{14}$ in 9:1 mol ratio were prepared (within a dry-room) by dissolving the lithium salt in the corresponding ionic liquid at 50 °C. Water content (determined by the standard Karl Fischer method using an automatic coulometer titrator Mettler Toledo DL32 located in dry-room) was <2 ppm in all samples and mixtures.

2.2. Viscosity and Conductivity Measurements. The viscosity measurements were carried out using a HAAKE RheoStress 600 rheometer located in a dry-room. The tests were performed from 20 to 80 °C (1 °C/min heating rate) in the 100 to 2000 s^{-1} rotation speed range. Viscosity values were taken in 10 °C steps. The ionic conductivity was determined by a conductivity meter AMEL 160. The binary mixtures were housed (in the dry-room) in sealed, glass conductivity cells (AMEL 192/K1) equipped with two porous platinum electrodes (cell constant equal to 1.0 ± 0.1 cm). The temperature was controlled by a climatic test chamber (Binder GmbH MK53). In order to fully freeze the sample mixtures,[26] the cells were immersed in liquid nitrogen for a few seconds and, then, transferred in the climatic chamber at −40 °C. After a few minutes of storage at this temperature, the solid samples turned again liquid. This route was repeated until the ionic liquid samples remained solid (at −40 °C). After a storage period at −40 °C for at least 18 hours, the conductivity was measured by running a heating scan at 1 °C h^{-1}.

2.3. NMR Measurements. The ^1H and ^{19}F NMR spectra were recorded on a Bruker Avance 500 spectrometer operating at 500 MHz proton frequency equipped with a QNP four nuclei switchable probe. The NMR samples were prepared in dry-room to avoid any contamination, transferred in a 5 mm NMR tube equipped with a coaxial capillary containing DMSO-d_6 for locking, and immediately flame-sealed. The DMSO-d_6 signal is also used as ^1H chemical shift reference. The ^{19}F chemical shifts were calibrated using exafluorobenzene as external reference heteronuclear $\{^1H-^{19}F\}$ and $\{^1H-^7Li\}$ HOESY experiments were acquired using the inverse-detected pulse sequence with 512 increments in the t1 dimension with 16 scans for each experiment and a mixing time of 40 ms. These NMR experiment were carried out at 28 °C.

Self-diffusion coefficients were measured by pulsed field gradient (PGSE) spin−echo experiments. A pulsed gradient unit capable of producing magnetic field pulse gradients in the *z*-direction of 53 G cm^{-1} was used, with the bipolar pulse longitudinal eddy current delay (BPPLED) pulse sequence. The ion self-diffusion coefficients were measured independently by carrying out experiments in the ^1H and ^{19}F frequency domains, respectively. The duration of the magnetic field pulse gradients (δ) and the diffusion times (Δ) were optimized for each sample in order to obtain complete dephasing of the signals with the maximum gradient strength. In each PGSE experiment, a series of 32 spectra with 16K points were collected. For the investigated samples, δ values were in the 1.5−3 ms while the Δ value was set to 1 s. The pulse gradients were incremented from 2 to 95% of the maximum value in a linear ramp. Temperature was varied within the range 27−67 °C in steps of 5 °C and controlled with an air flow of 535 L h^{-1}.

The ^7Li PGSE experiments were performed on a BRUKER AVANCE 200 spectrometer equipped with a MIC 200 MHz W2/S1 diff/30 probe with a gradient power of 1800 G/cm. The STE pulse sequence was used in the temperature range extending from 27 to 47 °C, controlled by water flow. The

Table 1. Experimental Self-Diffusion Coefficients D (m^2 s^{-1}) at 305 K and Activation Energies $E_a[D]$ (kJ/mol) for the Pure Ionic Liquids and the Mixtures $PYR_{14}TFSI/LiTFSI$, $PYR_{14}BETI/LiBETI$ and $PYR_{14}IM_{14}/LiIM_{14}$

ionic liquid	ion	D_{pure} [a,b]	D_{mix}	$E_a[D]_{pure}$ [a,b]	$E_a[D]_{mix}$
$PYR_{14}TFSI/LiTFSI$[a]	PYR_{14}^+	2.5×10^{-11}	1.7×10^{-11}	31	36
	$TFSI^-$	2.0×10^{-11}	1.2×10^{-11}	31	37
	Li^+		0.9×10^{-11}		46
$PYR_{14}BETI/LiBETI$	PYR_{14}^+	9.0×10^{-12}	6.2×10^{-12}	37	47
	$BETI^-$	6.2×10^{-12}	4.2×10^{-12}	37	48
	Li^+		2.3×10^{-12}		45
$PYR_{14}IM_{14}/LiIM_{14}$	PYR_{14}^+	6.4×10^{-12}	4.0×10^{-12}	43	51
	IM_{14}	4.3×10^{-12}	2.3×10^{-12}	43	51
	Li^+		1.6×10^{-12}		47

[a]Reference 14. [b]Reference 20.

ranges of the experimental parameters were δ = 2−3 ms and Δ = 0.08−0.035 s. In the temperature range of 52−67 °C, we used the dstegp3s sequence to avoid convection effects. In this sequence, SMSQ rectangular gradients were used with δ = 1 ms and Δ = 0.2−0.32 s. Temperature was controlled by an air flow of 800 l h^{-1}.

2.4. Computational Procedures. All calculations were performed with the B3LYP hybrid density functional and the 6-31G** basis set,[27] using the Gaussian 09 program.[28] The stable structures of the gas phase complexes $[Li(BETI)_2]^-$, $[Li(IM_{14})_2]^-$, and $[Li(TFSI)_2]^-$ were obtained in two sequential steps: (i) optimization of the anion geometries; (ii) formation of the complex by docking of the Li cation between two anions, followed by full energy minimization. Several starting orientations were used in the case of BETI, while two different starting geometries were used in the case of the IM_{14}-based complex. In the case of $[Li(TFSI)_2]^-$, we also performed relaxed potential energy scans by constraining one conformational degree of freedom and optimizing all the remaining ones. Further details are given below.

3. RESULTS AND DISCUSSION

3.1. Physical Properties. The self-diffusion coefficients D of the anions and cations in all samples were measured independently by PGSE experiments in the ^{19}F, ^1H, and ^7Li frequency domains, respectively. The observed echo intensity I is related to D and to the experimental parameters by the Stejskal-Tanner equation:[29]

$$I = I_0 \exp\left[-(\gamma g \delta)^2 D\left(\Delta - \frac{\delta}{3}\right)\right] \quad (1)$$

where I_0 is the echo intensity without field gradient, γ is the gyromagnetic ratio of the observed nucleus, g is the magnetic field gradient strength, δ is the duration of the gradient pulse, and Δ is the interval between the two pulses. The resulting self-diffusion coefficients at 305 K for the binary mixtures are reported in Table 1, alongside those for the TFSI-based mixtures from our previous work.[14]

It is interesting to compare the D values for the ions within the pure ILs and the mixtures. The general trend is $D(Li^+) < D(X^-) < D(PYR_{14}^+)$. This observation agrees with other literature data pertaining to Li-doped pyrrolidinium-[30−32] or imidazolium-[33−35] based ILs. It is generally admitted that the slower diffusion of the Li ions, compared with that of the bulkier pyrrolidinium ions, is a consequence of strong coordination of Li^+ to the anions, possibly leading to larger aggregates such as $[Li(X)_n]^{(n-1)-}$.[16,18] It is also interesting to note that the diffusion of the IL cation and anion is slowed by the addition of lithium. This parallels the IL viscosity increase caused by the lithium salts (see below).

The temperature dependency of the diffusion coefficients was investigated in the range T = 300−340 K. The results plotted in Figures 1 and 2 demonstrate that, within the explored temperature range, the diffusion coefficients follow the Arrhenius law:

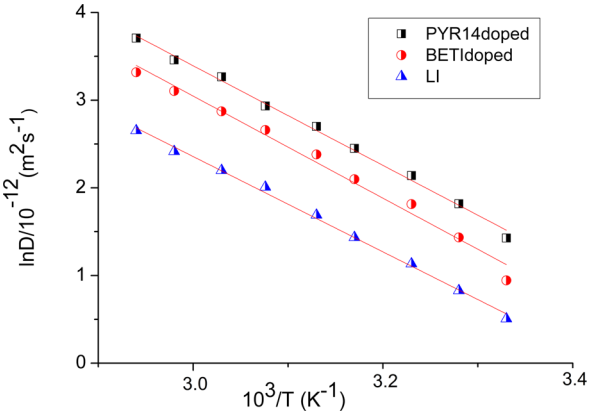

Figure 1. Arrhenius plot showing the temperature dependency of the ion diffusion coefficients in the ionic liquid mixtures $PYR_{14}BETI/LiBETI$.

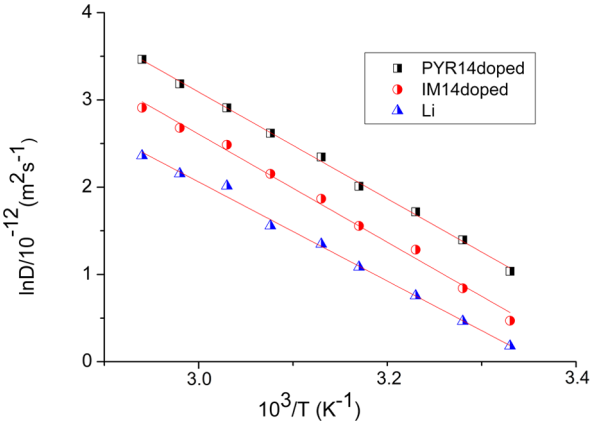

Figure 2. Arrhenius plot showing the temperature dependency of the ion diffusion coefficients in the ionic liquid mixtures $PYR_{14}IM_{14}/LiIM_{14}$.

$$D(T) = D_0 \exp(-E_a[D]/RT) \quad (2)$$

In all samples, the cation PYR_{14}^+ and the anion X^- have identical $E_a[D]$ values. The addition of LiX slows down the dynamics of both ions, increasing the activation energies for their motion but retaining identical values within each pair.[23]

The activation energy for the self-diffusion of Li^+ in all mixtures has a value of 46 ± 1 kJ mol^{-1}. This finding indicates that the mechanism of diffusion of Li^+ is different from that of the larger ions and is independent of the length of the anions' fluorinated chains. Thus, it seems that the key factor contributing to the activation energy for Li^+ diffusion is related to the presence, in all the examined anions, of the common perfluorosulfonylimide functional group.

The viscosities η, or equivalently the fluidities $\phi = \eta^{-1}$, were measured in the temperature range T = 293−373 K (Figure 3).

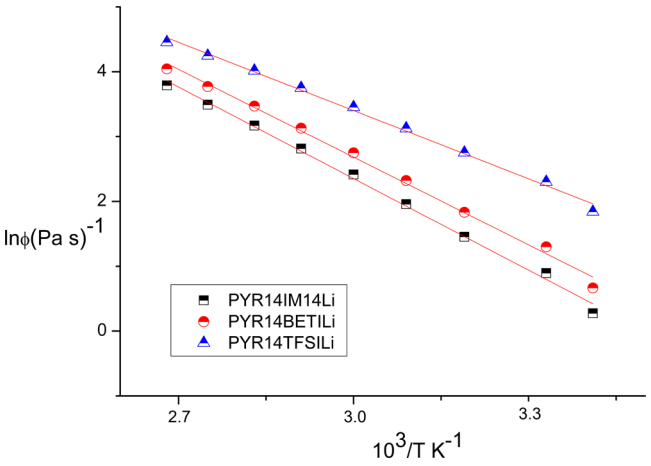

Figure 3. Arrhenius plot showing the temperature dependency of the fluidity in the ionic liquid mixtures PYR_{14}BETI/LiBETI and $PYR_{14}IM_{14}$/$LiIM_{14}$. The curve for PYR_{14}TFSI/LiTFSI is based on data of ref 14 and here reported for clarity.

These experimental data can also be fitted by the Arrhenius law and the corresponding activation energies $E_a[\phi]$ are reported in Table 2. The addition of the lithium salts produces a 50% reduction in fluidity but does not affect the corresponding activation energy. In this respect, the different behavior of the fluidities and the ion diffusion coefficients implies once again a breakdown of the Stokes−Einstein equation in ILs.[36] This is a consequence of the fact that these quantities describe collective and individual dynamical properties of the ions, respectively.

Table 2. Experimental Fluidities ϕ (Pa s)$^{-1}$ at 303 K and Activation Energies $E_a[\phi]$ (kJ/mol) for the Mixtures PYR_{14}TFSI/LiTFSI, PYR_{14}BETI/LiBETI, and $PYR_{14}IM_{14}$/$LiIM_{14}$ and for the Pure Compounds

ionic liquid	ϕ_{pure} [a,b]	ϕ_{mix} [a,b]	$E_a[\phi]_{pure}$ [a,b]	$E_a[\phi]_{mix}$
PYR_{14}TFSI/LiTFSI[a]	16.5	10.3	29	30
PYR_{14}BETI/LiBETI	5.0	3.6	36	37
$PYR_{14}IM_{14}$/$LiIM_{14}$	3.4	2.4	40	39

[a]Reference 14. [b]Reference 20.

The conductivities σ of the pure and doped samples are plotted in the Arrhenius form in Figure 4. We have not attempted to extract activation energies from these quantities, as they exhibit a clear non-Arrhenius behavior. This might be

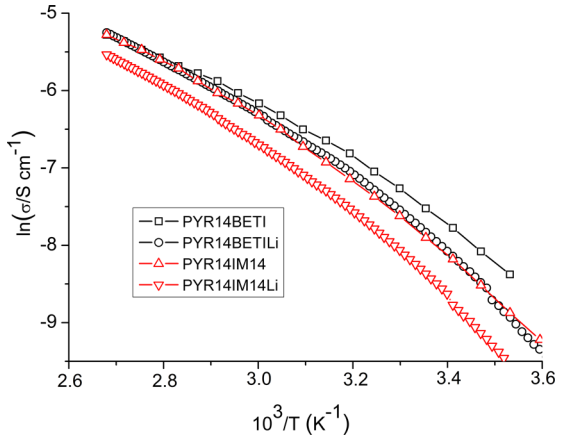

Figure 4. Arrhenius plot showing the temperature dependence of the conductivities of pure IL PYR_{14}BETI, $PYR_{14}IM_{14}$ and PYR_{14}BETI/LiBETI, $PYR_{14}IM_{14}$/$LiIM_{14}$ Li-doped mixtures.

due also to the fact that these quantities were measured in a wider temperature range, from 278 K (or lower) to 373 K. The Supporting Information presents the fits of these data according to the more general Vogel−Tammann−Fulcher law, which contains a reference temperature T_0 as an additional adjustable parameter. This temperature is found below 200 K, in all cases. From an applicative point of view, the important observation is that doping with lithium decreases the ionic conductivities of both ionic liquids, in agreement with previous observations.[24]

As a closing to this section, we briefly discuss the implications of these measurements for the Li-ion transport mechanism. Two distinct mechanisms have already been identified in the literature.[19] The "structure diffusion" mechanism (hopping of Li^+ from one coordination environment to another) necessarily involves a sizable activation energy for the breakup and formation of strong lithium-anion interactions. Instead, the competing "vehicular" mechanism (migration of Li^+ bound to its first coordination shell) implies a larger size of the diffusing species, but an activation energy comparable to that for the fluidity of the mixture. The fact that the measured activation energy for diffusion is significantly higher than that for fluidity clearly indicates that the first mechanism is more important than the second. Therefore, the computational part of our study was mainly focused on understanding the lithium-anion interactions and the mechanisms for the rearrangements within their coordination shells.

3.3. Theoretical Calculations. The measurements reported in the previous section demonstrate that the activation energies for Li-ion diffusion are independent of the length of the sulfonylimide anions' perfluorinated chains. Therefore, in order to understand this feature, it is natural to start from the simplest anion in the series, namely $TFSI^-$. This anion can exist in syn or anti conformations, depending on the relative arrangement of the terminal CF_3 groups (see Figure 5).[20−22] This also implies a different relative arrangement of the sulphonyl groups, so that the shortest O···O distance is 3.29 Å in the syn conformation and 2.89 Å in the anti one. According to our calculations, the latter is the most stable of the two, while the syn conformation is higher in energy by 3.26 kJ/mol. Analogous conformations were found also for the other anions, which, however, have additional degrees of freedom because of their longer perfluoroalkyl chains.

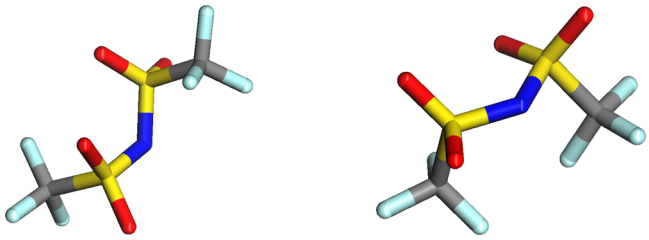

Figure 5. Anti (left) and syn (right) conformations of TFSI.

The interaction of the Li^+ cation with the fluorinated anions was investigated by optimizing the structure of $[Li(X)_2]^-$ model aggregates. Our calculations on the $[Li(TFSI)_2]^-$ aggregate show that the more stable configurations contain Li^+ tetrahedrally coordinated by four oxygen atoms, as shown in Figure 6. Recent experimental and computational work on TFSI/FSI mixtures of pyrrolidinium-based[18] or closely related[20−22] ILs at variable Li^+ content confirmed that the Li-ion coordination strongly depends on the mixture composition and that, for the 9:1 mol ratio examined in the present paper, the Li cation is surrounded by 4 oxygen atoms in its first coordination shell. The most stable complex (structure a) contains both anions in the anti conformation. Next, in order of increasing energy, we have structure b at +6.8 kJ/mol, in which one anion is anti and the other is syn. Structure c has both anions in a syn conformation (+14.1 kJ mol^{-1}). The fact that the energy of the O-coordinated complexes increases by 7 kJ mol^{-1} when an anti conformation is replaced by a syn one, whereas the energy of an isolated anion increases by slightly more than 3 kJ mol^{-1}, indicates that the Li-anion interaction is more favorable in the anti conformation. Indeed, we find that an anion in the anti state can readily coordinate Li^+ (the intramolecular O···O distance is 2.88 Å, virtually identical to that in the isolated anion), whereas an anion in the syn state can chelate Li^+ only at the cost of some intramolecular distortion.

When Li^+ is coordinated by the two nitrogen atoms of the anion, the energy of the $[Li(TFSI)_2]^-$ aggregate rises to more than 60 kJ/mol with respect to the absolute minimum (structure d in Figure 6). Thus, coordination of Li^+ by the nitrogens can be ruled out. This point is in agreement with the single crystal X-ray structures previously reported.[37] This might appear surprising, considering that these atoms are negatively charged. The preference for the interaction with the oxygen atoms may be understood in terms of the Lewis concepts of hardness and softness. Because of its small size, Li^+ is a very hard acid, which interacts more favorably with O (hard Lewis base) than with the softer N^- moiety.

On the basis of these findings, we have approached the minimization of the $[Li(BETI)_2]^-$ complex. Figure 7 illustrates two minima, with energies differing only by 0.54 kJ mol^{-1}. In both configurations, the Li^+ cation is tetrahedrally coordinated by four oxygen atoms, and the state of the central portions of the molecules resembles that in the anti/syn complex of TFSI (structure b) in Figure 6.

Starting geometries for the $[Li(IM_{14})_2]^-$ complex were generated with all-trans, extended conformations of the perfluorobutyl chains. As shown in Figure 8, which displays the final equilibrium geometries, the anions' chains could be either roughly parallel or roughly antiparallel (a and b, respectively). The latter, antiparallel structure has a slightly higher energy of +2.83 kJ mol^{-1}. Once more, the Li^+ cation is tetrahedrally coordinated by four oxygen atoms belonging to two anions. Thus, the lithium first coordination shell is not influenced by the length of the anion's fluorinated chains.

Going back to the simplest aggregate, the $[Li(TFSI)_2]^-$ complex, we have calculated the energetic requirements of two types of rearrangement, which may be correlated to the "structure diffusion" mechanism for the migration of the Li cation. We have calculated the potential energy curves associated with a deformation along two structural coordinates. Coordinate α corresponds to the dihedral angle formed by atoms 1−2−3−4 in Figure 9a and therefore involves the concerted replacement of a Li^+−O bond by another one. Coordinate β corresponds to the dihedral angle formed by atoms 1−2−3−4 in Figure 9b and therefore involves the passage through a roughly square-planar coordination of the

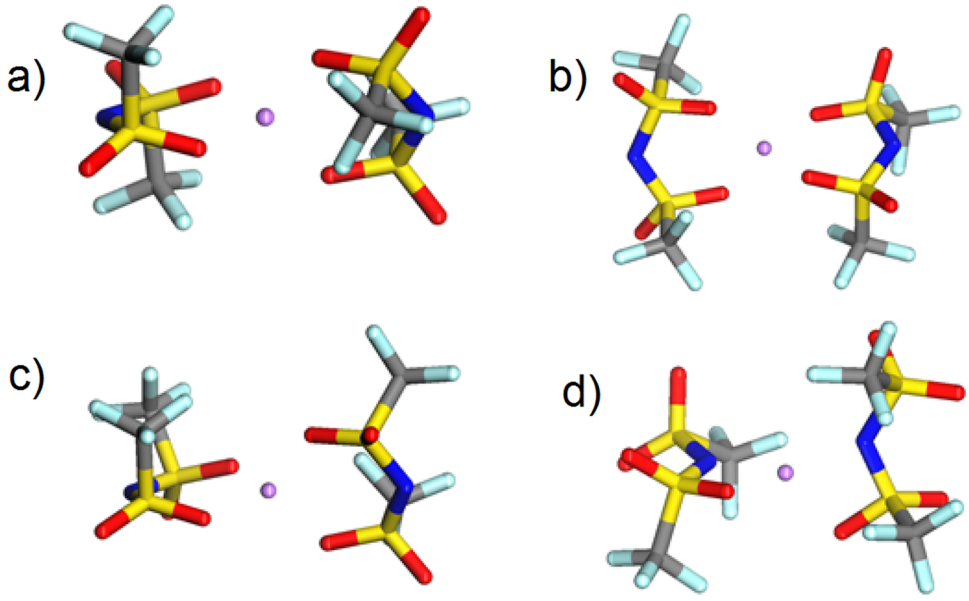

Figure 6. Minimized structures of the $[Li(TFSI)_2]^-$ complex.

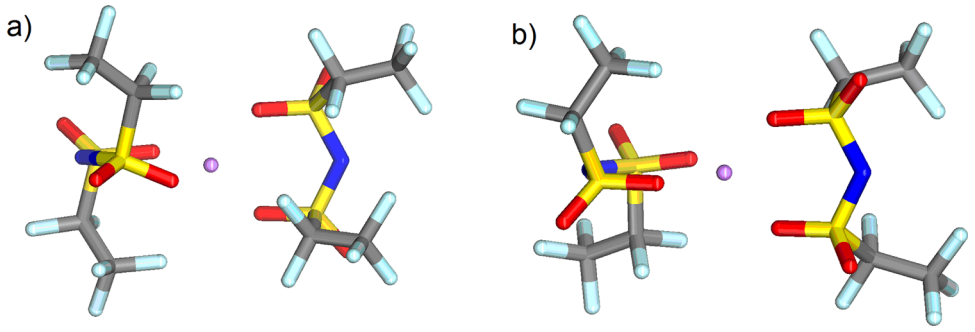

Figure 7. Minimum energy structures of the $[Li(BETI)_2]^-$ complex.

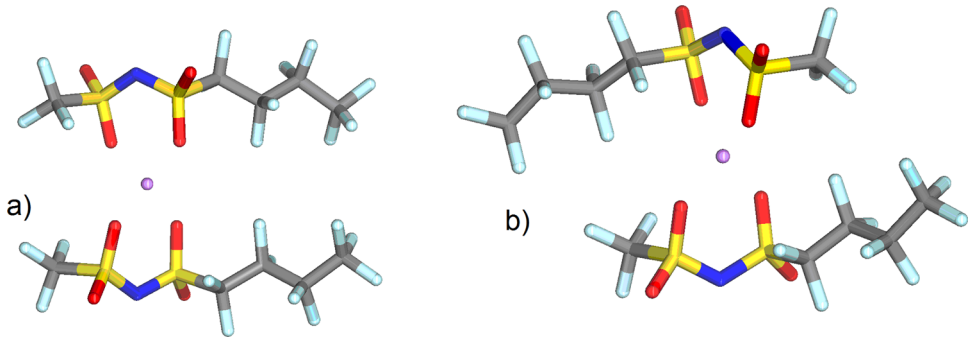

Figure 8. Minimum energy structures of the $[Li(IM_{14})_2]^-$ complex.

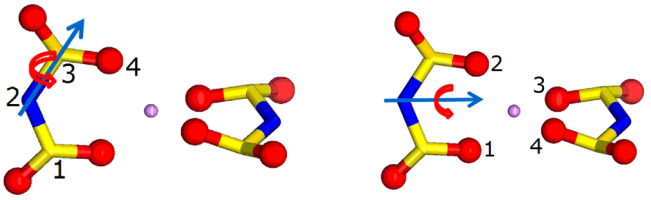

Figure 9. Definition of the dihedral angles α (left) and β (right), scanned by B3LYP/6-31G** calculations on the $[Li(TFSI)_2]^-$ complex. The terminal CF_3 groups are not shown, for clarity.

cation. Starting from the absolute minimum (structure a in Figure 6), we changed these coordinates in 10° steps, and at each point we reoptimized the structure while keeping α or β fixed. Figure 10 shows that the potential barriers for both types of rearrangement are of the order of 50 kJ mol^{-1}, in agreement with the experimental activation energy for Li^+ diffusion in the ILs considered in this study. This result provides two important indications. First, the rearrangement of the tetrahedrically coordinated Li cage with the sulfonylimide ligands makes a significant contribution to the transition state for the Li-ion diffusion mechanism, thus confirming the importance of the structure diffusion scheme. Second, the remote, dangling perfluorocarbon substituents can be expected to provide only a small, if not negligible, contribution to the energy profile along the reaction coordinate, in agreement with the NMR data.

3.4. Intermolecular Contacts via Nuclear Overhauser Enhancements. For the two $PYR_{14}X/LiX$ samples (X= BETI or IM_{14}) as well as for the pure $PYR_{14}X$ ILs, high-resolution ^1H, ^{19}F, and ^7Li NMR spectra could be obtained at room temperature, despite the high viscosity of the solution (spectra

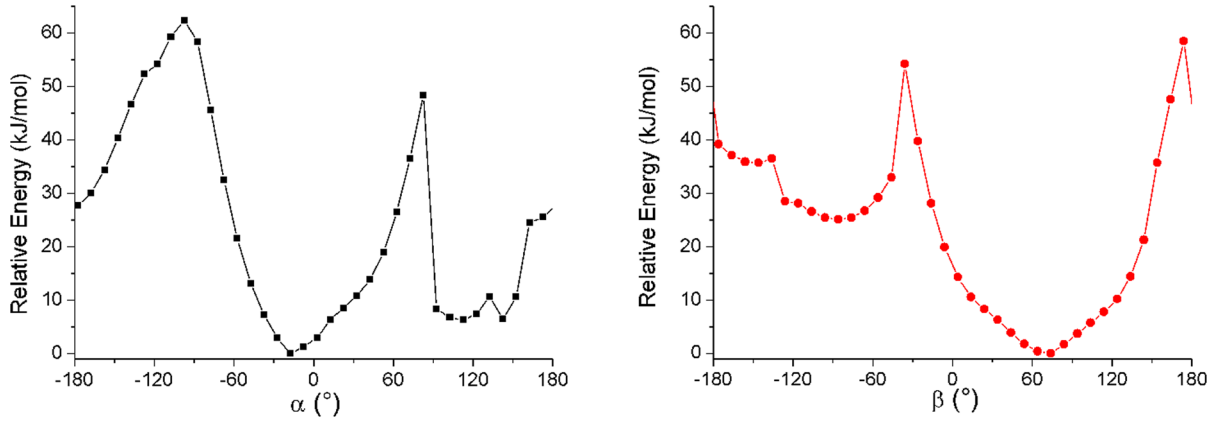

Figure 10. B3LYP/6-31G** potential energy curves along the dihedral angles α (squares, left) and β (circles, right) defined in Figure 9. The minimum energy conformation has $\alpha = -17.45°$ and $\beta = 73.13°$.

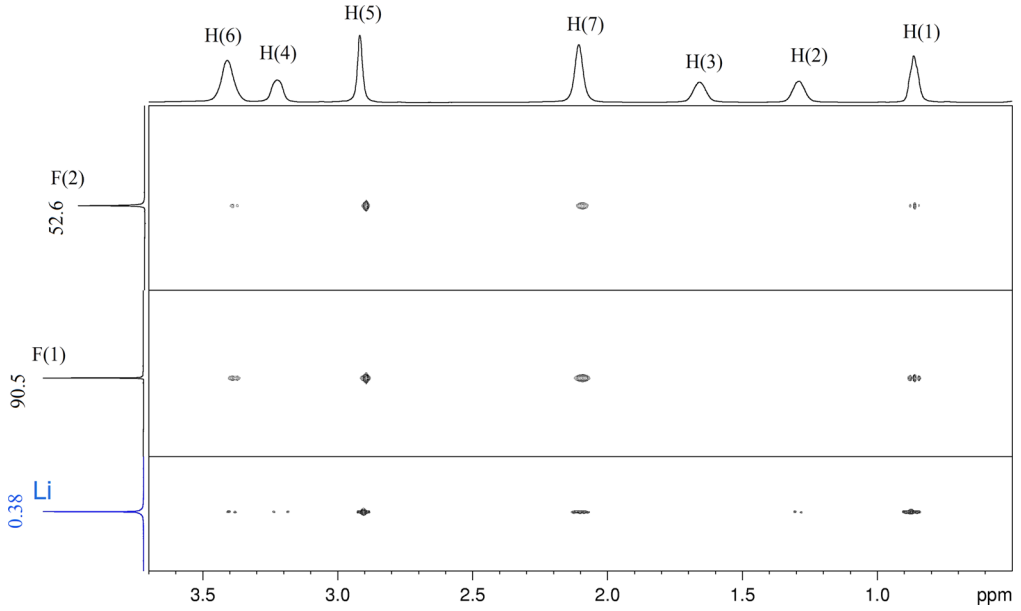

Figure 11. Contour plot of {^{1}H–^{19}F} (top) and {^{1}H–^{7}Li} (bottom) HOESY spectrum of $PYR_{14}BETI/LiBETI$. ^{7}Li and ^{19}F chemical shifts are reported for clarity. See the Experimental Section for referencing.

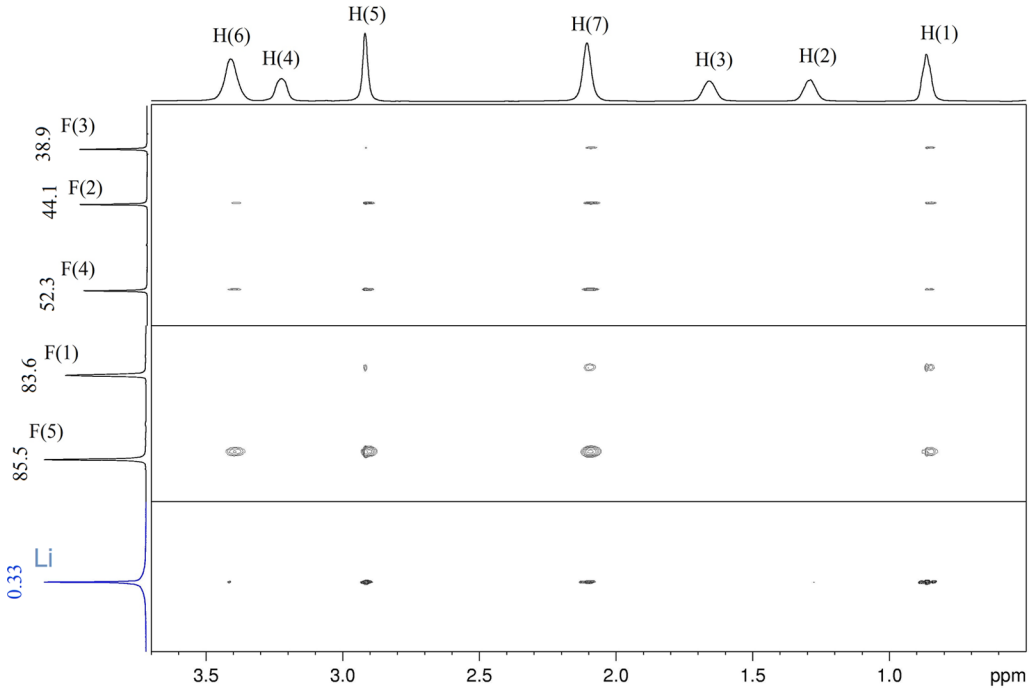

Figure 12. Contour plot of {^{1}H–^{19}F} (top) and {^{1}H–^{7}Li} (bottom) HOESY spectrum of $PYR_{14}IM_{14}/LiIM_{14}$. ^{7}Li and ^{19}F chemical shifts are reported for clarity. See the Experimental Section for referencing.

reported in the SI). The sharpness of the NMR peaks for all of these species, and for 0.10 LiTFSI/0.90 PYR_{14}TFSI in ref 14, is dramatically different from that reported by Frömling et al.[30] for the 0.377 LiTFSI/0.623 PYR_{14}TFSI system, where broad bands without fine structure were observed for all nuclei. The difference is likely due to the higher viscosity of the latter, due to its much higher Li content. We stress that, on the basis of our previous studies, the present concentrations are near-optimal for practical lithium battery applications.[38]

For our system, no chemical shift differences induced by LiX dopant are observed in the ^{1}H spectra with respect to the undoped reference (Figure S1). Similarly, only small chemical shift differences are observed in the ^{19}F spectra of the pure and doped $PYR_{14}BETI$ samples (Figure S2). The ^{7}Li NMR spectra of $PYR_{14}BETI/LiBETI$ and $PYR_{14}IM_{14}/LiIM_{14}$ (Figure S3) consist of a single, sharp peak showing a small chemical shift difference. The sharpness of the Li signal (line width 8 Hz) is interesting, considering the quadrupolar nature of this nucleus (I = 3/2). This indicates a highly symmetric environment, with near-zero electric field gradient, in agreement with the tetrahedral coordination of Li^{+}.

As previously reported, useful information for the assessment of the structure of ionic liquids can be obtained from the NMR HOESY correlation spectroscopy.[39,40] However, the interpre-

tation of intermolecular NOEs requires special attention,[23,41−43] as the intermolecular cross-relaxation may include long-range effects usually not present in the intramolecular case, where the R^{-6} decay law of the NOE intensity with the distance R between the I and S interacting nuclei renders the NOE intensity negligible beyond the 5 Å threshold. This concept was recently formally developed in a mathematical model for cross-relaxation in ionic liquids by Gabl, Steinhauser, and Weingärtner (GSW).[44,45] The basic concept is that the distance dependence of intermolecular NOE strongly depends on the $(\omega_I - \omega_S)$ difference of the Larmor frequencies of the interacting nuclei. A practical consequence of this finding is that the R^{-6} short-range dependence, strictly true for the intramolecular cross-relaxation, turns into a more general R^{-n} law, with $n < 6$. Consequently, long-range effects are likely to be detected in intermolecular NOE experiments whenever the frequencies of the cross-relaxing nuclei are close, as in the $\{^1H-^1H\}$, $\{^1H-^{19}F\}$, and, to a much lesser extent, $\{^1H-^7Li\}$ cases. Therefore, the GSW model imposes a careful interpretation of intermolecular NOE data, including long-range effects. At the same time, it offers the possibility of an unprecedented comparison of NOE data with structural parameters obtained by small-angle X-ray and neutron scattering, as recently stressed.[46]

Figures 11 and 12 show the expansion of the HOESY experiments carried out on the $PYR_{14}BETI/LiBETI$ and $PYR_{14}IM_{14}/LiIM_{14}$ mixtures. The NMR absorption peaks are numbered according to Scheme 1. The $\{^1H-^{19}F\}$ NOE data

Scheme 1. Molecular Formula and Atom Numbering of the PYR_{14}^+ Cation (Left) with the $TFSI^-$, $BETI^-$, and IM_{14}^- Anions (Right, from Top to Bottom)

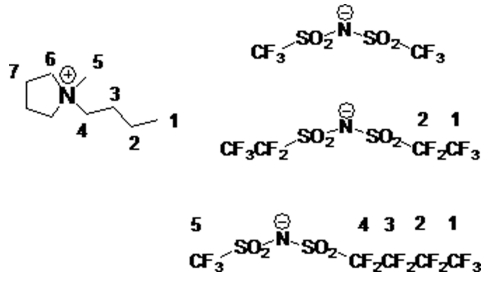

show the dipolar contacts between the protons of PYR_{14}^+ and the fluorine nuclei of anions, while the $\{^1H-^7Li\}$ NOE correlation spectrum gives information on the dipolar interactions of the Li^+ dopant with the PYR_{14}^+ components of the mixture.

Before commenting on the results on the doped systems, we point out that $\{^1H-^{19}F\}$ HOESY spectra of the pure compounds $PYR_{14}BETI$ and $PYR_{14}IM_{14}$ showed selective NOE contacts between the fluorines of the anion and the H(6), H(7), H(5), and H(1) protons belonging to the pyrrolidinium ring and the methyl groups of the cation, while no interaction with the inner protons of the butyl chain was observed.[20] The $PYR_{14}BETI/LiBETI$ sample has a $\{^1H-^{19}F\}$ NOE pattern which is very similar to that of the pure IL. This, together with the absence of chemical shift differences among the samples, indicates that the majority of cation−anion interactions are not affected by doping. Intriguingly, the $\{^1H-^7Li\}$ NOE spectrum shows an analogous selectivity of the Li^+ cations toward the protons of PYR_{14}^+. In particular, there is a strong NOE between Li^+ and H(5), H(7), and the remote H(1). This result suggests that Li^+ ions do have short contacts with PYR_{14}^+, despite the presence of a positive charge on both species. A straightforward rationale for the observed $\{^1H-^7Li\}$ NOE can be proposed by remembering that Li^+ is strongly coordinated to the anions giving rise to negatively charged complexes, such as $[Li(X)_2]^-$ (X = TFSI, BETI, IM_{14}). These Li-containing aggregates thus undergo Coulombic interaction with the PYR_{14} cations. The selective NOE patterns also point out that such an interaction is specific and not random, leading to an organized picture of the Li^+ solvation shells. The importance of the Li^+-anion binding is further confirmed by the similarity between the NOE patterns of the lithium and fluorine nuclei with the PYR_{14}^+ cation, despite their obvious chemical differences: indeed, Li^+ and the perfluorinated anions experience the same distribution of cations in the closest solvation spheres.

This conclusion holds also for the $PYR_{14}IM_{14}/LiIM_{14}$ sample. The heteronuclear NOE experiments (Figure 12) show patterns similar to those of $PYR_{14}BETI/LiBETI$. The NOE data confirm the Li^+-anion coordination, even in the presence of longer perfluorocarbon substituents attached to the sulfonylimide core. Again, the strong coordination of Li^+ with the IL anions is responsible for the spatial proximity of Li^+ and PYR_{14}^+ cation, irrespective of the presence of Coulombic repulsion. The contour plots of Figure 12 shows strong NOE contacts of both the CF_3 groups of IM_{14}, namely F(5) and F(1), with the terminal methyl group of the PYR_{14}^+ butyl chain. The presence of these NOE correlations indicates cross-relaxation beyond the first solvation sphere. Such data can only be interpreted by invoking the GSW model for intermolecular NOE patterns in ILs.

4. CONCLUSIONS

We have presented a comparative physicochemical study of two ionic liquids $PYR_{14}X$ (X= BETI or IM_{14}) doped with the LiX salts in the 9:1 molar ratio. Ion diffusion coefficients and viscosity data have been collected over a range of temperatures and they show an Arrhenius-like temperature dependence. The strong changes in the activation energies for these processes, together with further conductivity data (which have a non-Arrhenius behavior), indicate that doping with lithium produces a strong perturbation in the microscopic dynamics of the ions. DFT calculations have allowed us to better define the structure of the environment of Li^+, which has been found to be coordinated to four oxygen atoms originating from two anions. The energy barriers calculated for the rearrangement of this coordination are comparable to the measured activation energies for lithium diffusion (about 46 kJ mol^{-1}, independently of the anion's perfluorinated chain length). Although modeling the transition state(s) for the diffusive jumps of Li^+ is well beyond the purpose of this work, these calculation confirm the predominance of the "structure diffusion" over the "vehicular" mechanism of lithium transport. Finally, the heteronuclear, intermolecular NOE data have been interpreted in light of the recent GSW model.[44,45] The NOE data not only confirm the Li-anion coordination as the major structural feature in these systems but also shed light on the interactions of the butyl and perfluorobutyl moieties. Further work is in progress on a larger variety of alkyl and perfluoroalkyl homologues in order to assess the possible formation of multiple domains (e.g., polar, nonpolar, and fluorophilic) on the nanometer scale, as previously suggested for other IL systems.[46]

ASSOCIATED CONTENT

Supporting Information

^{1}H, ^{19}F, and ^{7}Li NMR spectra of the pure IL and their mixtures. Results of the Vogel−Tammann−Fulcher fits of the conductivities. This material is available free of charge via the Internet at http://pubs.acs.org.

AUTHOR INFORMATION

Corresponding Author

*E-mail: andrea.mele@polimi.it. Ph.: +39-02-23993006. Fax: +39-02-23993180.

Notes

The authors declare no competing financial interest.

ACKNOWLEDGMENTS

The authors acknowledge the EU for funding (FP7, GREENLION Project, Contract No. 285268) and the support of Regione Lombardia and CILEA Consortium through a LISA Initiative 2013 grant (Laboratory for Interdisciplinary Advanced Simulation: http://lisa.cilea.it).

REFERENCES

(1) Castner, E. W., Jr.; Wishart, J. F. Spotlight on Ionic Liquids. *J. Chem. Phys.* **2010**, *132*, 120901/1−120901/9.

(2) Ueno, K.; Tokuda, H.; Watanabe, M. Ionicity in Ionic Liquids: Correlation with Ionic Structure and Physicochemical Properties. *Phys. Chem. Chem. Phys.* **2010**, *12*, 1649−1658.

(3) Weingartner, H. Understanding Ionic Liquids at the Molecular Level: Facts, Problems and Controversies. *Angew. Chem., Int. Ed.* **2008**, *47*, 654−670.

(4) Ott, D.; Kralisch, D.; Stark, A. In *Handbook of Green Chemistry*; Anastas, P., Ed.; Wiley & Sons: New York, 2010; Vol. 6, p 315.

(5) Plechkova, N. V.; Seddon, K. R. Applications of Ionic Liquids in the Chemical Industry. *Chem. Soc. Rev.* **2008**, *37*, 123−150.

(6) Torimoto, T.; Tsuda, T.; Okazaki, K.-I.; Kuwabata, S. New Frontiers in Materials Science Opened by Ionic Liquids. *Adv. Mater.* **2010**, *22*, 1196−1221.

(7) Armand, M.; Endres, F.; MacFarlane, D. R.; Ohno, H.; Scrosati, B. Ionic-Liquid Materials for the Electrochemical Challenges of the Future. *Nat. Mater.* **2009**, *8*, 621−629.

(8) Tarascon, J.-M.; Armand, M. Issues and Challenges Facing Rechargeable Lithium Batteries. *Nature* **2001**, *414*, 359−367.

(9) Shin, J. H.; Henderson, W. A.; Passerini, S. PEO-Based Polymer Electrolytes with Ionic Liquids and Their Use in Lithium Metal-Polymer Electrolyte Batteries. *J. Electochem. Soc.* **2005**, *152*, A978−A983.

(10) Hayashi, K.; Nemoto, Y.; Akuto, K.; Sakurai, Y. Alkylated Imidazolium Salt Electrolyte for Lithium Cells. *J. Power Sources* **2005**, *146*, 689−692.

(11) Takada, A.; Imaichi, K.; Kagawa, T.; Takahashi, Y. Abnormal Viscosity Increment Observed for an Ionic Liquid by Dissolving Lithium Chloride. *J. Phys. Chem. B* **2008**, *112*, 9660−9662.

(12) Rosol, Z. P.; German, N. J.; Gross, S. M. Solubility, Ionic Conductivity and Viscosity of Lithium Salts in Room Temperature Ionic Liquids. *Green Chem.* **2009**, *11*, 1453−1457.

(13) Umecky, T.; Saito, Y.; Okumura, Y.; Maeda, S.; Sakai, T. Ionization Condition of Lithium Ionic Liquid Electrolytes Under the Solvation Effect of Liquid and Solid Solvents. *J. Phys. Chem. B* **2008**, *112*, 3357−3364.

(14) Castiglione, F.; Ragg, E.; Mele, A.; Appetecchi, G. B.; Montanino, M.; Passerini, S. Molecular Environment and Enhanced Diffusivity of Li^+ Ions in Lithium-Salt-Doped Ionic Liquid Electrolytes. *J. Phys. Chem. Lett.* **2011**, *2*, 153−157.

(15) Nicolau, B. G.; Sturlaugson, A.; Fruchey, K.; Ribeiro, M. C. C.; Fayer, M. D. Room Temperature Ionic Liquid−Lithium Salt Mixtures: Optical Kerr Effect Dynamical Measurements. *J. Phys. Chem. B* **2010**, *114*, 8350−8356.

(16) Borodin, O.; Smith, G. D.; Henderson, W. Li^+ Cation Environment, Transport, and Mechanical Properties of the LiTFSI Doped N-Methyl-N-alkylpyrrolidinium$^+$ $TFSI^-$ Ionic Liquids. *J. Phys. Chem. B* **2006**, *110*, 16879−16886.

(17) Monteiro, M. J.; Bazito, F. F. C.; Sequeira, L. J. A.; Ribeiro, M. C. C.; Torresi, R. M. Transport Coefficients, Raman Spectroscopy, and Computer Simulation of Lithium Salt Solutions in an Ionic Liquid. *J. Phys. Chem. B* **2008**, *112*, 2102−2109.

(18) Tsuzuki, S.; Hayamizu, K.; Seki, S.; Ohno, Y.; Kobayashi, Y.; Miyashiro, H. Quaternary Ammonium Room-Temperature Ionic Liquid Including an Oxygen Atom in Side Chain/Lithium Salt Binary Electrolytes: Ab Initio Molecular Orbital Calculations of Interactions between Ions. *J. Phys. Chem. B* **2008**, *112*, 9914−9920.

(19) Lersch, V.; Jeremias, S.; Moretti, A.; Passerini, S.; Heuer, A.; Borodin, O. A Combined Theoretical and Experimental Study of the Influence of Different Anion Ratios on Lithium Ion Dynamics in Ionic Liquids. *J. Phys. Chem. B* **2014**, *118*, 7367−7375.

(20) Lassègues, J.-C.; Grondin, J.; Aupetit, C.; Johansson, P. Spectroscopic Identification of the Lithium Ion Transporting Species in LiTFSI-Doped Ionic Liquids. *J. Phys. Chem. A* **2008**, *113*, 305−314.

(21) Umebayashi, Y.; Mori, S.; Fujii, K.; Tsuzuki, S.; Seki, S.; Hayamizu, K.; Ishiguro, S. Raman Spectroscopic Studies and Ab Initio Calculations on Conformational Isomerism of 1-Butyl-3-methylimidazolium Bis-(trifluoromethanesulfonyl)amide Solvated to a Lithium Ion in Ionic Liquids: Effects of the Second Solvation Sphere of the Lithium Ion. *J. Phys. Chem. B* **2010**, *114*, 6513−6521.

(22) Fujii, K.; Hamano, H.; Doi, H.; Song, X.; Tsuzuki, S.; Hayamizu, K.; Seki, S.; Kameda, Y.; Dokko, K.; Watanabe, M.; Umebayashi, Y. Unusual Li^+ Ion Solvation Structure in Bis(fluorosulfonyl)amide Based Ionic Liquid. *J. Phys. Chem. C* **2013**, *117*, 19314−19324.

(23) Castiglione, F.; Moreno, M.; Raos, G.; Famulari, A.; Mele, A.; Appetecchi, G. B.; Passerini, S. Structural Organization and Transport Properties of Novel Pyrrolidinium-Based Ionic Liquids with Perfluoroalkyl Sulfonylimide Anions. *J. Phys. Chem. B* **2009**, *113*, 10750−10759.

(24) Castiglione, F.; Raos, G.; Appetecchi, G. B.; Montanino, M.; Passerini, S.; Moreno, M.; Famulari, A.; Mele, A. Blending Ionic Liquids: How Physico-Chemical Properties Change. *Phys. Chem. Chem. Phys.* **2010**, *12*, 1784−1792.

(25) Appetecchi, G. B.; Tizzani, C.; Scaccia, S.; Alessandrini, F.; Passerini, S. Synthesis of Hydrophobic Ionic Liquids for Electrochemical Applications. *J. Electrochem. Soc.* **2006**, *153*, A1685−A1691.

(26) Henderson, W. A.; Passerini, S. Phase Behaviour of Ionic Liquids-LiX Mixtures: Pyrrolidinium Cations and $TFSI^-$ Anions. *Chem. Mater.* **2004**, *16*, 2881−2885.

(27) Koch, W.; Holthausen, M. C. *A Chemist's Guide to Density Functional Theory*; Wiley-VCH: Weinheim, Germany, 1999.

(28) Frisch, M. J.; et al. Gaussian 09, Revision D.01; Gaussian, Inc.: Wallingford, CT, 2009.

(29) Callaghan, P. T. *Principles of Nuclear Resonance Microscopy*; Oxford University Press: Oxford, U.K., 1991.

(30) Frömling, T.; Kunze, M.; Schönhoff, M.; Sundermeyer, J.; Roling, B. Enhanced Lithium Transference Numbers in Ionic Liquid Electrolytes. *J. Phys. Chem. B* **2008**, *112*, 12985−12990.

(31) Rollet, A.-L.; Bessada, C. Chapter Four − NMR Studies of Molten Salt and Room Temperature Ionic Liquids. *Annu. Rep. NMR Spectrosc.* **2013**, *78*, 149−207.

(32) Nicotera, I.; Oliviero, C.; Henderson, W. H.; Appetecchi, G. B.; Passerini, S. NMR Investigation of Ionic Liquid−LiX Mixtures: Pyrrolidinium Cations and $TFSI^-$ Anions. *J. Phys. Chem. B* **2005**, *109*, 22814−22819.

(33) Niu, S.; Cao, Z.; Li, S.; Yan, T. Structure and Transport Properties of the $LiPF_6$ Doped 1-Ethyl-2,3-dimethyl Imidazolium Hexafluorophosphate Ionic Liquids: A Molecular Dynamics Study. *J. Phys. Chem. B* **2010**, *114*, 877−881.

(34) Saito, Y.; Umecky, T.; Niwa, J.; Sakai, T.; Maeda, S. Existing Condition and Migration Property of Ions in Lithium Electrolytes with Ionic Liquid Solvent. *J. Phys. Chem. B* **2007**, *111*, 11749−11802.
(35) Duluard, S.; Grondin, J.; Bruneel, J.-L.; Pianet, I.; Grélard, A.; Campet, G.; Delville, M.-H.; Lassègues, J.-C. Lithium Solvation and Diffusion in the 1-Butyl-3-methylimidazolium bis-(trifluoromethanesulfonyl)imide Ionic Liquid. *J. Raman Spectrosc.* **2008**, *39*, 627−632.
(36) Taylor, A. W.; Licence, P.; Abbott, A. P. Non-Classical Diffusion in Ionic Liquids. *Phys. Chem. Chem. Phys.* **2011**, *13*, 10147−10154.
(37) Zhou, Q.; Boyle, P. D.; Malpezzi, L.; Mele, A.; Shin, J.-H.; Passerini, S.; Henderson, W. A. Phase Behavior of Ionic Liquid−LiX Mixtures: Pyrrolidinium Cations and $TFSI^-$ Anions − Linking Structure to Transport Properties. *Chem. Mater.* **2011**, *23*, 4331−4337.
(38) Appetecchi, G. B.; Montanino, M.; Passerini, S., Ionic Liquid-based Electrolytes for High-Energy Lithium Batteries in *Ionic Liquids: Science and Applications*, ACS Symposium Series 1117, Vissser, A. E., Bridges, N. J., Rogers, R. D., Eds.; Oxford University Press, Inc., American Chemical Society: Washington, DC, 2013.
(39) Lingscheid, Y.; Arenz, S.; Giernoth, R. Heteronuclear NOE Spectroscopy of Ionic Liquids. *ChemPhysChem* **2012**, *13*, 261−266.
(40) Bankmann, D.; Giernoth, R. Magnetic Resonance Spectroscopy in Ionic Liquids. *Prog. Nucl. Magn. Reson. Spectrosc.* **2007**, *51*, 63 −90.
(41) Halle, B. Cross-Relaxation between Macromolecular and Solvent Spins: The Role of Long-Range Dipole Couplings. *J. Chem. Phys.* **2003**, *119*, 12372−12385.
(42) Frezzato, D.; Rastrelli, F.; Bagno, A. Nuclear Spin Relaxation Driven by Intermolecular Dipolar Interactions: The Role of Solute−Solvent Pair Correlations in the Modeling of Spectral Density Functions. *J. Phys. Chem. B* **2006**, *110*, 5676−5689.
(43) Mele, A. NOE Experiments for Ionic Liquids. Tools and Strategies. *Chim. Oggi/Chem. Today* **2010**, *28*, 48−55.
(44) Gabl, S.; Steinhauser, O.; Weingärtner, H. From Short-Range to Long-Range Intermolecular NOEs in Ionic Liquids: Frequency Does Matter. *Angew. Chem., Int. Ed.* **2013**, *52*, 9242−9246.
(45) Gabl, S.; Schroeder, C.; Braun, D.; Weingärtner, H.; Steinhauser, O. Pair Dynamics and the Intermolecular Nuclear Overhauser Effect (NOE) in Liquids Analysed by Simulation and Model Theories: Application to an Ionic Liquid. *J. Chem. Phys.* **2014**, *140*, 184503−184515.
(46) Russina, O.; Lo Celso, F.; Di Michiel, M.; Passerini, S.; Appetecchi, G. B.; Castiglione, F.; Mele, A.; Caminiti, R.; Triolo, A. Mesoscopic Structural Organization in Triphilic Room Temperature Ionic Liquids. *Faraday Discuss.* **2013**, *167*, 499−513.